Subproject F2.1

Nanostructured Functional Layers for Advanced Oxygen Separation Membranes

Principle Investigators: Dagmar Gerthsen and Ellen Ivers-Tiffée

CFN-Financed Scientists: Levin Dieterle (1/2 BAT IIa, 18 months), Baicheng Pei (45 % BAT IIa, 18 months),

Further Scientists: Dr. Mónica Burriel, Philipp Müller, Christian Niedrig, Dr. Heike Störmer, Simon Taufall, Dr. Stefan Wagner

Laboratorium für Elektronenmikroskopie (LEM)
Institut für Werkstoffe der Elektrotechnik (IWE)

Karlsruhe Institute of Technology (until Oct. 2009: Universität Karlsruhe (TH))

Nanostructured Functional Layers for Advanced Oxygen Separation Membranes

1. Introduction

The reduction or elimination of CO_2 emissions is a major issue for the present and future: Electrical power plants fueled by coal or gas produce CO_2 emissions which have to be reduced by 50 to 60 % by 2050, as mandated by the European Commission. For oxyfuel combustion, the focus is on the generation of pure oxygen from air by means of oxygen separation techniques. This mission can be achieved by making use of membrane technology, an approach that can be considered energetically favourable as compared to cryogenic methods. After combustion of the fuel in pure oxygen, the resulting CO_2 can be taken care of by established carbon capture and storage (CCS) techniques.

For an application as dense ceramic oxygen-transport membranes (OTM), mixed ionic-electronic conducting (MIEC) solid oxides are of great interest, given their excellent oxygen-ionic and electronic transport properties, resulting in both high oxygen permeability and selectivity for oxygen/air separation in the targeted temperature range (~ 800 °C). Very promising oxides are those of the perovskite (ABO_3) type, a structure that combines great flexibility and chemical stability, thus permitting custom-tailoring of the materials properties by doping the A or B sites with different elements and stoichiometries. In this way, the composition $Ba_{0.5}Sr_{0.5}Co_{0.8}Fe_{0.2}O_{3-\delta}$ (henceforth denoted BSCF) was found to exhibit very high permeation fluxes [1;2]. In related joint research projects focusing on the oxygen-permeation properties of MIEC materials for OTM applications, such as the Helmholtz Alliance MEM-BRAIN, BSCF has hence been identified as most promising candidate.

However, there is little knowledge about the long-term structural and electrochemical stability under application-relevant temperatures. In addition to the cubic perovskite phase with high oxygen-ion conductivity [1;3;4], a hexagonal [5;6] and a “plate-like” phase, most probably consisting of alternating cubic/hexagonal BSCF layers [7] were already detected in BSCF. Therefore, further investigations concerning the stability and further performance optimization are required.

In general, there is a strong demand for an enhancement of OTM performance (increasing oxygen flux), in particular rate-limiting surface exchange kinetics between gas phase and solid oxide, e.g., by nanoscale surface modification. The main target of subproject F2.1 is the investigation of the advantageous effect of nanostructured functional layers on the solid oxygen transport through a dense ceramic membrane. Corresponding preliminary studies on related MIEC perovskite materials have shown promising results, either by depositing nanoporous films of the same material (resulting in an increased electrochemically active surface area), or of a different material enabling a faster oxygen exchange. To this end, however, a thorough analysis of the underlying basic material properties (electrochemistry and phase stability under operating conditions) of BSCF is a prerequisite and has therefore been a key part of the work performed within the first part of the funding period.

2. Sample Fabrication

One major goal of the project is to determine accurate values for the chemical oxygen surface exchange coefficient k^{δ}, since it determines the overall performance of the material as oxygen separation membrane. To-date, all studies of oxygen transport in BSCF (e.g., [8-10]) have focused on polycrystalline samples. However, as the sample morphology strongly affects the transport

properties of polycrystalline samples, with issues not related to electrochemistry, such as particle size, grain boundary shape, connectivity, or porosity, becoming influential, the intrinsic transport parameters of BSCF are difficult to extract. Therefore, dense epitaxial BSCF layers were fabricated in the course of this study. In addition, pulsed-laser deposition (PLD) was applied in collaboration with the group of José Santiso at the Centro de Investigación en Nanociencia y Nanotecnologia, CIN2 (CSIC-ICN), in Bellaterra/Spain as well as with the Institut für Festkörperphysik (IFP) at KIT. $NdGaO_3$ (110) (NGO) single crystal substrates and (110) $(LaAlO_3)_{0.3} - (SrAl_{0.5}Ta_{0.5}O_3)_{0.7}$ (LSAT) single crystal substrates were chosen to promote an epitaxial growth of the layers. LSAT is a commonly used substrate material for the epitaxial growth of a variety of perovskite PLD layers. On the other hand, the orthorhombic NGO with pseudo-cubic in-plane parameters of 3.863 and 3.854 Å exhibits a small mismatch with the basal plane of the cubic BSCF perovskite structure (cell parameter of 3.983 Å [11]). Furthermore, NGO is basically electrically insulating (conductivity $\sigma_{NGO,\ 700\ °C} \approx 10^{-6}$ S/cm << $\sigma_{BSCF,\ 700\ °C} \approx 10^{+2}$ S/cm) and inert to oxygen exchange, thus being an ideal substrate for electrical and electrochemical investigations of the deposited BSCF thin-films.

Prior to PLD, the single phase perovskite of the BSCF target material was confirmed by X-ray diffraction (XRD). The expected stoichiometric composition was confirmed by X-Ray fluorescence. Ablation was performed by using a KrF excimer laser (UV light pulses- $\lambda = 248$ nm) with a 10 Hz repetition rate. The energy density per pulse at the target site amounted to 3 J/cm^2. The substrate temperature was fixed to 700 °C with an oxygen pressure of 0.4 mbar. By applying different numbers of pulses, ranging from 4000 to 10000, BSCF film thicknesses between 140 and 340 nm were realized. In Figure 1, an SEM micrograph of an epitaxial PLD-BSCF film on NGO is given. As can be seen, completely dense and crack-free BSCF films with quite flat surfaces were realized.

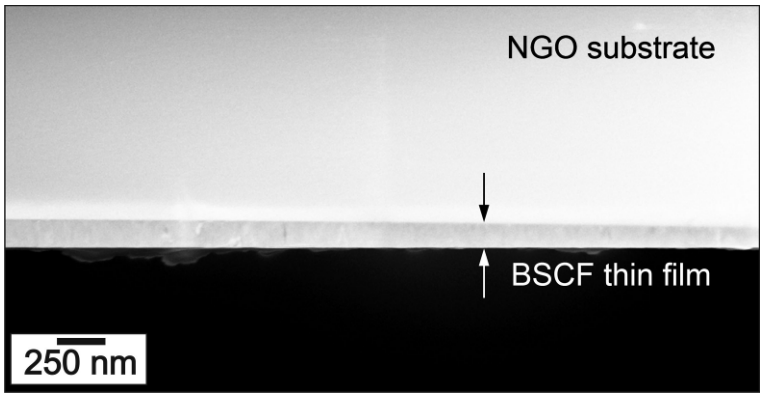

Figure 1: Cross-sectional SEM micrograph of an as-deposited BSCF PLD thin film (thickness ~ 150 nm) on a $NdGaO_3$ (110) substrate showing a homogeneous, completely dense layer without any signs of delamination.

3. Electrochemical Characterization

A major parameter determining the oxygen transport in an OTM material is its chemical oxygen surface exchange coefficient k^{δ}. Diffusion losses within the material can be minimized (and, thus, higher oxygen fluxes obtained) by reducing the OTM thickness (e.g., by using a supported membrane structure consisting of a dense electrochemically active thin film on a porous substrate); however, upon reducing the thickness below a certain value, oxygen surface transfer will become rate-determining for the oxygen permeation rate. For thin films, the oxygen permeation rate will thus be controlled by the oxygen exchange coefficient of the material. Hence, knowledge of k^{δ} values is essential. To-date, all studies of oxygen transport in BSCF (e.g., [8-10]) have focused on

polycrystalline samples. Here, we focus on dense, epitaxial BSCF thin films, thus aiming at the intrinsic material properties, unperturbed by any morphological influences.

The electrical properties of BSCF epitaxial films on NGO substrates (and of BSCF bulk samples) have been measured in pure oxygen and in air atmosphere in the temperature range from 40 to 900 ºC. In Fig. 2 the total conductivity of a thin-film sample measured in air has been plotted vs. the temperature. For comparison, conductivity values obtained from bulk sample measurements both from own work and from literature data have been added. In both cases (thin film and bulk sample) the conductivity of BSCF increases with temperature, presenting a semiconductor-type behavior corresponding to a small polaron hopping mechanism, associated with the behavior of mixed ($3^+/4^+$) valence states of Co and Fe cations.

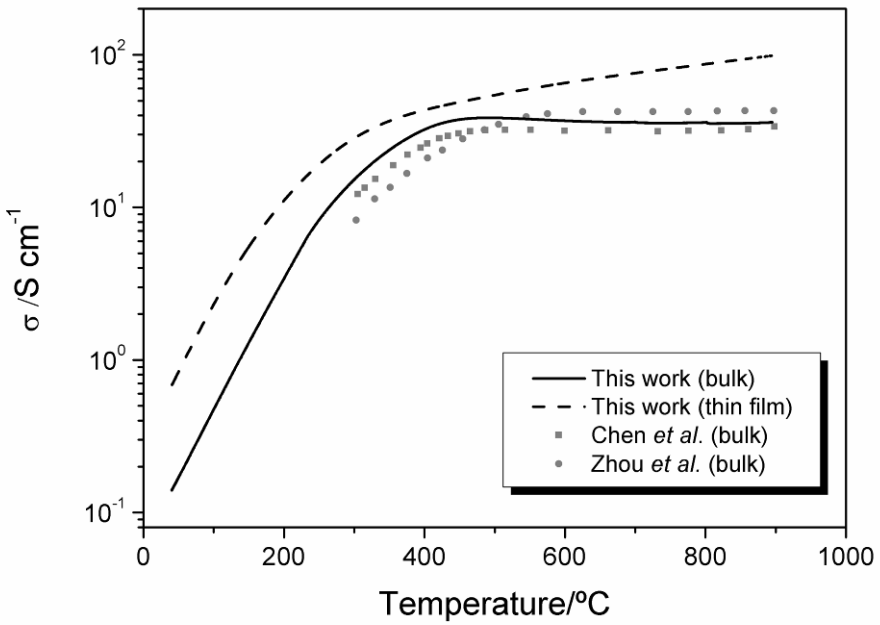

Figure 2: Total conductivity of BSCF bulk samples and epitaxial films (340 nm thickness) in air as a function of temperature and comparison with literature data [9;10].

It can be observed that the behavior of the BSCF bulk sample matches the data published by other authors for BSCF polycrystalline samples [9;10], whereas the thin film performs slightly differently. Firstly, the overall conductivity of the epitaxial thin film is significantly higher in the whole investigated temperature range. Moreover, in the case of the bulk samples, the conductivity increases with temperature up to approximately 400 ºC, then reaching a plateau. At high temperatures the creation of additional oxygen vacancies, accompanied by a reduction of Fe^{4+} to Fe^{3+} or Co^{4+} to Co^{3+}, causes a decrease in the charge carrier concentration and a covalent interaction because of a perturbation of the O–(Fe,Co)–O periodic potential, which may account for such a transition [10]. In the case of the thin film a similar behavior is found at low temperatures, while at high temperatures the conductivity does not reach a maximum, but continues slightly increasing in the whole temperature range. This could be due to differences in the oxygen vacancy content and defects equilibration. Considering that the conductivity curve deviation at higher temperatures is only related to the loss of oxygen by surface exchange, then the oxidation enthalpy seems to be considerably reduced in thin films compared to that in bulk material, which could be related to the strain induced by the substrate and/or to the crystallographic orientation of the surface planes.

Figure 3 shows the results of k^{δ} values obtained by a frequency-domain analysis of electrical conductivity relaxation (ECR) data of two epitaxial BSCF films with thicknesses of 340 nm in a fast oxygen pressure modulation setup. To confirm a good reproducibility of the measurements, each of the samples was measured in cycles, first heating and then cooling, maintaining a plateau at each temperature to ensure equilibration before the measurement. The temperature cycles were repeated between 2 and 4 times for each of the samples. The activation energy of the surface exchange process is calculated to 93 kJ/mol. The values published in literature for k^{δ} by the ECR technique have been measured for temperatures higher than 600 ºC but by measuring the conductivity relaxation in the frequency domain, the measuring temperature range could be extended down to 400 ºC. The k^{δ} rate constants measured for the dense thin films in the high temperature range are of the same order of magnitude of those measured by Girdauskaite et al. [12], and approximately half an order of magnitude lower compared to those measured by Bucher et al. [13] for polycrystalline BSCF samples. (The activation energy of the process has an intermediate value between those measured by these two groups.)

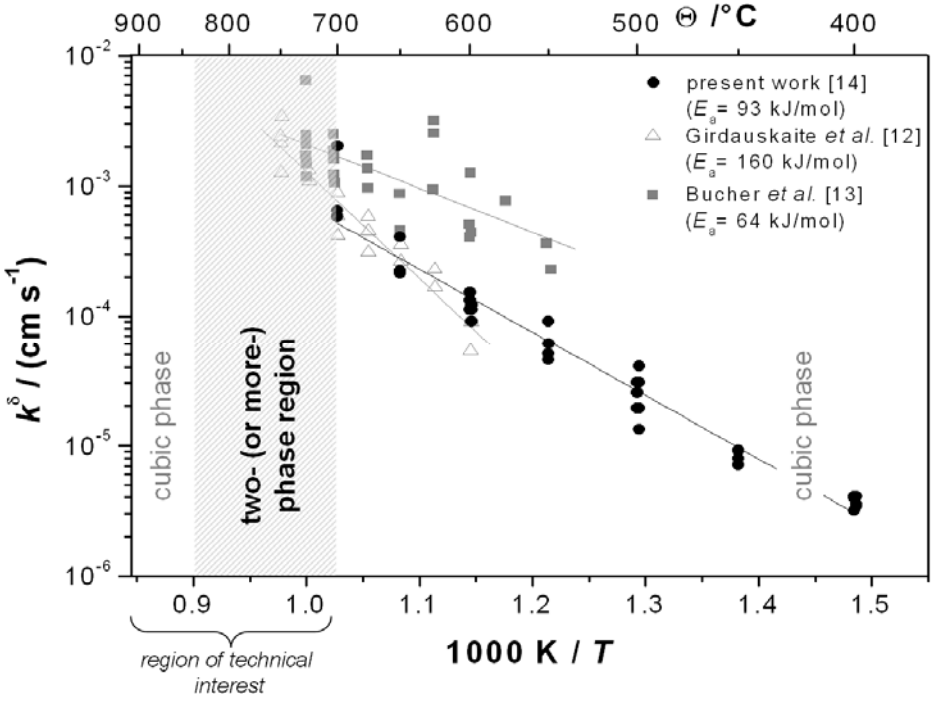

Figure 3: Oxygen surface exchange coefficients k^{δ} for epitaxial BSCF thin films on NGO substrate obtained in synthetic air [14] compared to literature values for BSCF bulk samples [12;13]. The shaded area indicates a temperature range where the single-phase cubic BSCF system is not stable.

As can be seen from Figure 4, the BSCF PLD samples undergo severe phase changes after treatment at temperatures above 700 °C during measurements. In the next section, these phenomena will be highlighted by microstructural analyses. As the kinetic measurements are very sensitive to changes in the surface morphology, electrochemical measurements performed on thin-film samples above this temperature do not give accurate information about the properties of the cubic BSCF phase.

4. Microstructural Characterization

To exploit the full potential of the BSCF material, the knowledge of phase composition and stability of the cubic BSCF phase is of key interest. It is known [5] that the cubic BSCF phase decomposes in the targeted operation temperature range (~ 800 °C) which degrades the electrical conductivity

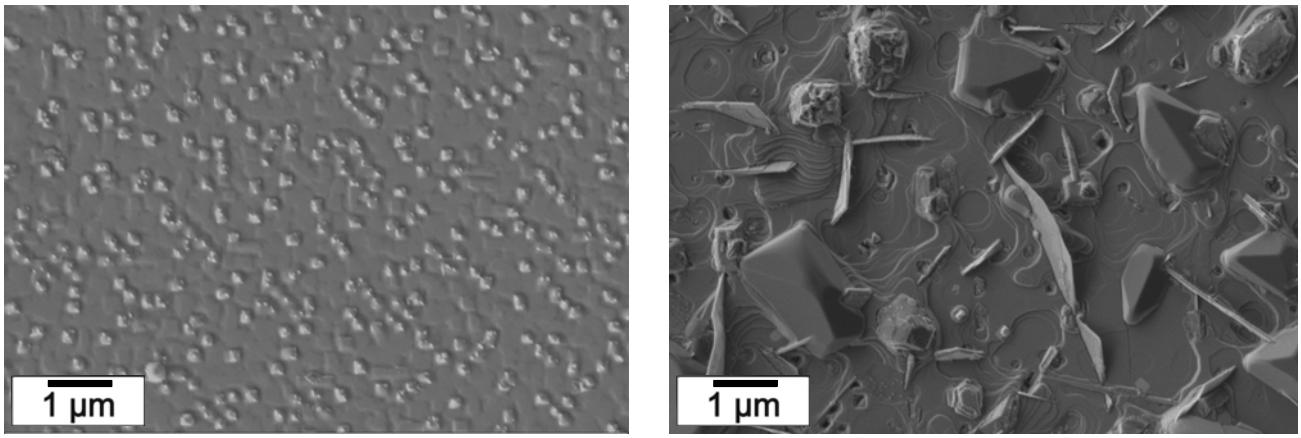

Figure 4: SEM micrographs of epitaxial BSCF PLD thin films (on NGO) after deposition at 700 °C (left) and after several days of annealing in the temperature range from 700...900 °C (right).

To obtain more information on phase stability, XRD analyses were carried out on BSCF powders, instead of thin films, due to the higher resolution and lack of detrimental influence of the substrate. To this end commercially available BSCF powder supplied by the Fraunhofer Institute for Ceramic Technologies and Systems (IKTS), Hermsdorf/Germany ($D_{50} \approx 2.40$ µm) was used.

Moreover, detailed microstructural characterization was performed on both thin BSCF layers fabricated by pulsed-laser deposition (PLD) on LSAT substrates as well as BSCF bulk samples. The investigation of bulk samples facilitates the study of the stability of BSCF under application-relevant conditions with respect to phase transitions. The BSCF bulk samples were fabricated from the aforementioned BSCF powder by uniaxial pressing, followed by sintering at 1000 °C for 12 h. Further annealing at application-relevant temperature (800 °C) was performed for up to 1350 h.

Figure 5 shows the results of an XRD analysis performed on a BSCF powder sample that was annealed in ambient air at 800 °C. Multiple subsequent XRD analyses were performed after heat treatment for 72 h, 120 h, 240 h, 600 h and 1680 h, respectively. This was realized by holding the powder sample at 800 °C for the desired time – followed by a cooling procedure (20 K/min) and subsequent XRD pattern recording – and heating up to 800 °C again. In Figure 3, the formation of a hexagonal BSCF phase from the initially pure cubic powder (a) can be observed. Already after 72 h annealing, hexagonal reflections – corresponding to the (101), (201) and (112) planes – are clearly detectable in the XRD pattern.

The single-phase cubic perovskite raw powder has a lattice constant of 3.986 Å, which corresponds well to the values determined by other groups, e.g. [5;11]. All nine reflections in the 2Θ-range from 20° to 80° were fitted using WinINDEX (Bruker AXS) which yields only one possible result with a figure of merit (FoM) of 363. A similar WinINDEX fit to the hexagonal peaks ranging from 2Θ-range from 20° to 80° yields hexagonal lattice constants $a = b = 5.629$ Å and $c = 4.361$ Å, in good agreement with the values determined, e.g., by [5].

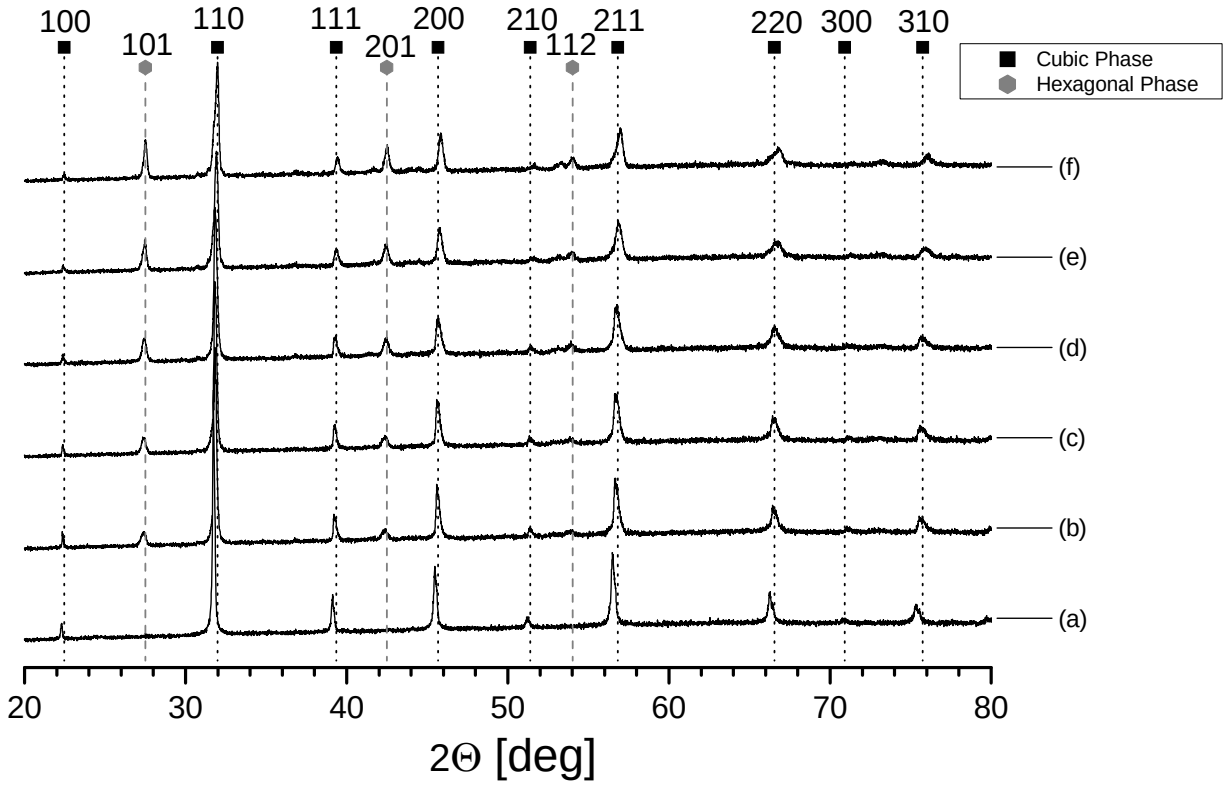

Figure 5: XRD spectra of BSCF raw powder (a) and after annealing at 800 °C in ambient air for 72 h (b), 120 h (c), 240 h (d), 600 h (e) and 1680 h (f), showing a continuous increase of the reflections from the hexagonal (101), (201) and (112) plane [15].

With increasing annealing time, the hexagonal reflections continue to gain in intensity. By a quantitative analysis of the peak intensities (integrated counts), the formation of the hexagonal phase in BSCF powder was found to occur following an exponential growth mechanism with a t_{90} value of approximately 45 days. These findings, which can be related to a long-term conductivity degradation observed in bulk samples by the authors [15], are in good agreement with recent observations on the phase growth in bulk samples reported in literature [16].

However, the information regarding the phase composition based solely on XRD is naturally restricted. Thus, with respect to recent literature suggesting a more intricate phase composition of BSCF [6;7], a comprehensive characterization by electron microscopy is necessary to gain deeper insight into the decomposition of the cubic BSCF phase under operation-relevant conditions.

Detailed microstructural characterization of the phase composition was performed employing transmission electron microscopy (TEM) in combination with convergent-beam electron diffraction (CBED) and energy-dispersive X-ray spectroscopy (EDXS). Figure 6 shows cross-section bright-field images of a thin BSCF layer on an LSAT substrate, annealed at 800 °C for 10 h in air after PLD deposition. The cubic BSCF layer with a thickness of about 50 nm is single-crystalline and epitaxially oriented with respect to the substrate. Plate-like crystallites approximately 20 nm in width and up to 150 nm in length and with a different crystal structure are embedded in the layer. The occurrence of an additional phase indicates the decomposition of the cubic phase at 800 °C.

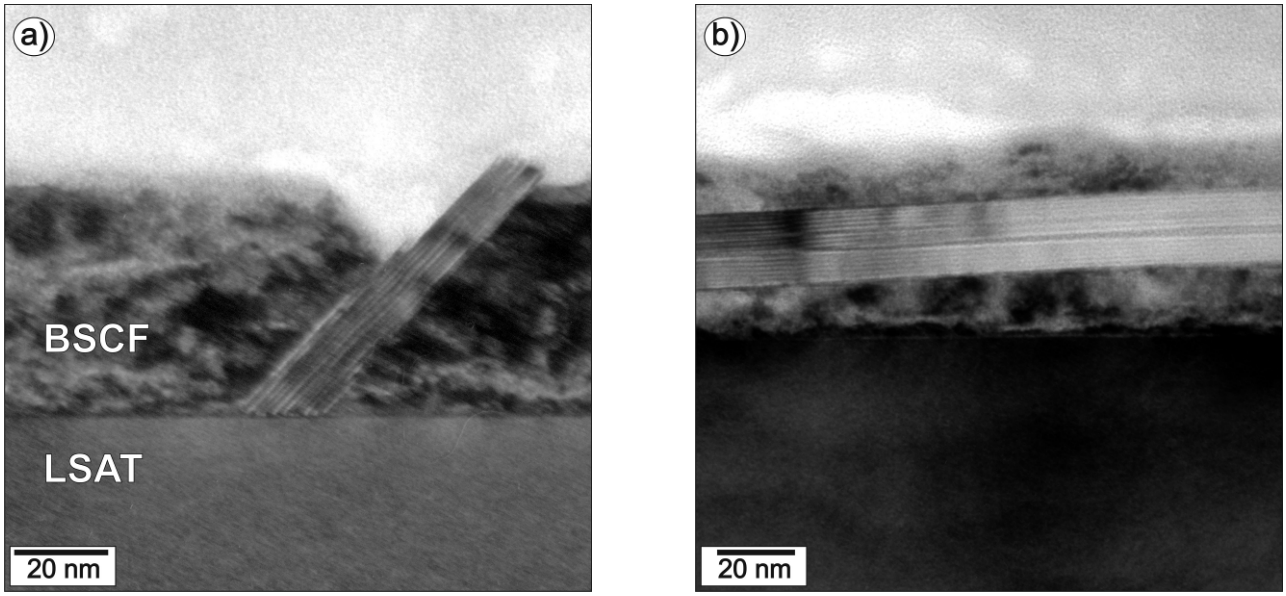

Figure 6: Cross-section TEM bright-field images of a BSCF thin-film on LSAT, annealed at 800 °C for 10 h/air after PLD. Plate-like crystallites, approximately 20 nm in width and up to 150 nm in length are observed in the BSCF layer.

EDXS was performed to determine the chemical composition of the "plate-like" phase. Figure 7(b) shows the cation concentrations determined by an EDXS line-scan across a plate-like crystallite. The region of the line-scan is indicated by the grey bar in the scanning transmission electron microscopy (STEM) image Fig. 7(a).

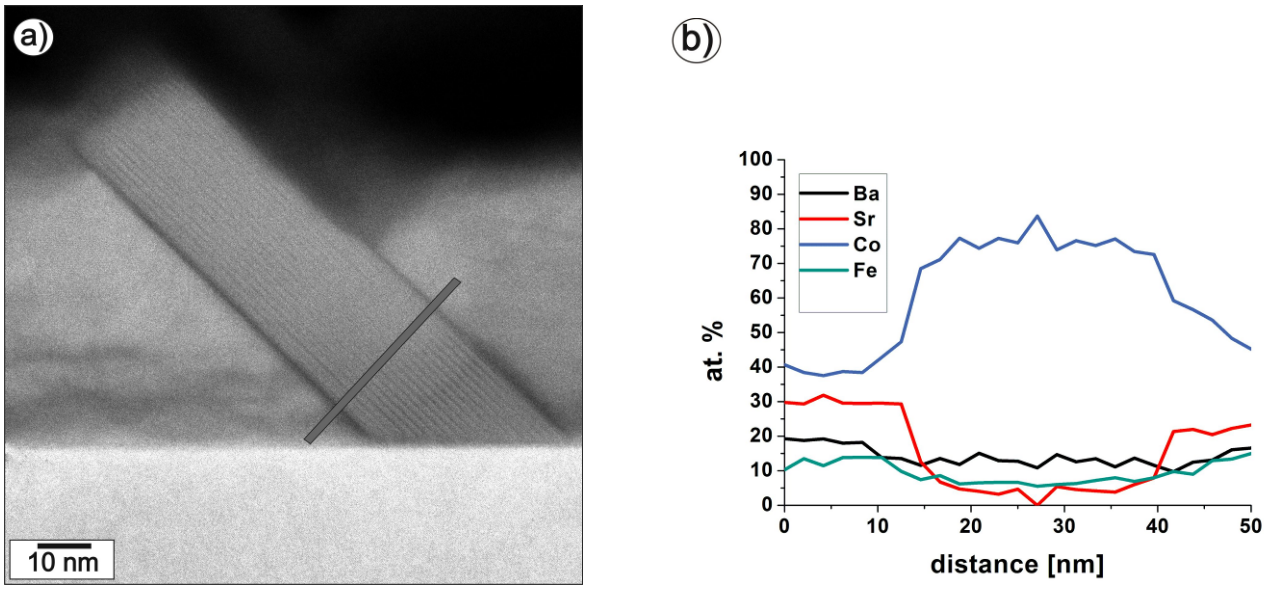

Figure 7: EDXS line-scan across one plate-like crystallite within a BSCF thin-film sample. (a) The region of the scan is indicated by a grey bar in the STEM image; (b) Ba-, Sr-, Co-, Fe-concentrations in atomic percent plotted as a function of distance.

The EDXS analysis reveals a significant Sr-depletion and Co-enrichment in the plate-like crystallite. The amount of barium and iron remains unchanged within the accuracy of measurement. On the left side of the EDXS scan, the Sr-signal is slightly enhanced compared to the right end of the scan. This is an artifact of measurement in the vicinity of the LSAT substrate which also contains Sr cations.

To analyze the decomposition of the cubic phase under application-relevant conditions in detail, BSCF bulk samples were annealed at different temperatures (700 °C – 1000 °C) for different periods of time. Details about bulk-sample fabrication are given in [17]. Figure 8 shows a bright-field TEM image of a BSCF bulk sample annealed at 800 °C for 1350 h. Grains consisting of three different phases are marked in the micrograph. The phase assignment is based on chemical analyses by EDXS and selected-area electron diffraction (SAED).

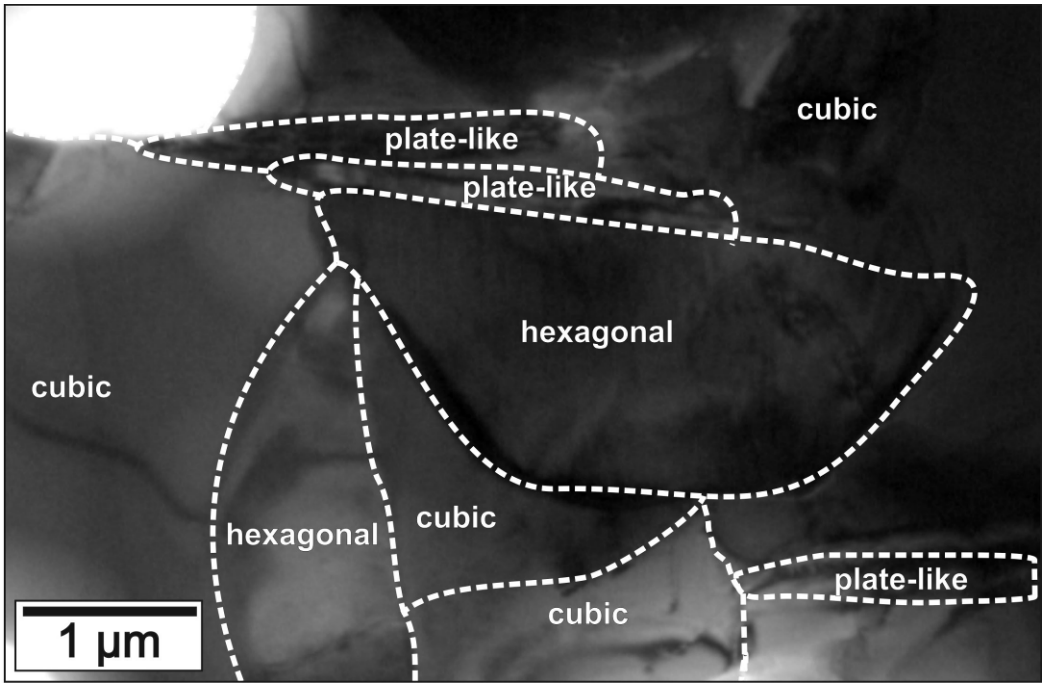

Figure 8: Bright-field TEM image of BSCF annealed at 800 °C for 1350 h. Three different phases were found by selected-area electron diffraction.

In addition to the cubic phase, a hexagonal phase is observed, which was already detected by XRD [15,18]. In addition, plate-like crystallites are observed which are similar to the precipitates in the BSCF layers after annealing at 800 °C. This confirms that the plate-like crystallites are formed due to cubic-phase decomposition, and not as an artifact of the PLD layer fabrication. The SAED patterns of the "plate-like" phase cannot be interpreted on the basis of the cubic and hexagonal crystal structures.

The chemical composition of grains in the BSCF bulk samples, representing the different crystalline phases, was determined by EDXS. The cation contents (at. %) are given in Table 1. The cubic BSCF phase is characterized by a cation ratio Ba:Sr:Co:Fe ~ 5:5:8:2 in good agreement with the intended composition. However, the "plate-like" and hexagonal phase contain different cation concentrations. The "plate-like" phase is characterized by a strong excess of B-site cations (cobalt) while the Sr-content is depleted. In contrast, the hexagonal phase shows an increased amount of A-site cations. We also note that the composition of the cubic phase in the vicinity of the plate-like

crystallites does not show compositional deviations compared to the cubic matrix within the accuracy of the measurement.

Composition [at. %]	**Ba**	**Sr**	**Co**	**Fe**
Cubic BSCF	26 ± 1.5	23 ± 2.0	40.5 ± 1.5	10.5 ± 1.0
"Plate-like" phase	21.5 ± 1.5	2.5 ± 1.0	67 ± 1.0	9 ± 1.0
Hexagonal phase	30.5 ± 0.5	24.0 ± 1.0	43.5 ± 1.0	2 ± 0.5

Table 1: Chemical composition of the different phases observed in the BSCF bulk samples. The values are given in atomic percent of the total cation content. The errors are the standard deviations of all sample regions under investigation exhibiting the given phase.

Convergent beam electron diffraction (CBED) was used for investigations of the crystal-structure symmetry of the "plate-like" phase. CBED is well suited for this purpose because it allows imaging of higher order Laue-zones (HOLZ) [20] which yield three-dimensional crystal structure information. Figures 9 and 10 show CBED patterns of the "plate-like" and hexagonal phase in the zone axis with the highest symmetry.

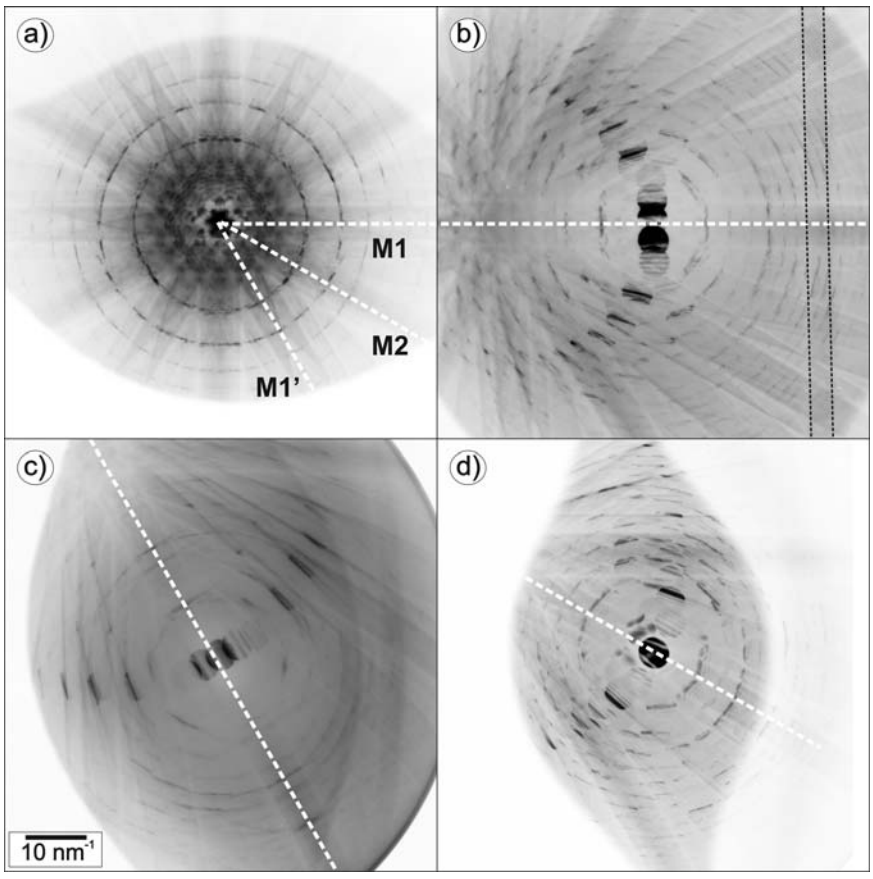

Figure 9: CBED patterns of the "plate-like" phase. The field of view was extended by tilting the sample along the direction of the symmetry planes (M1, M2) indicated by dashed lines.

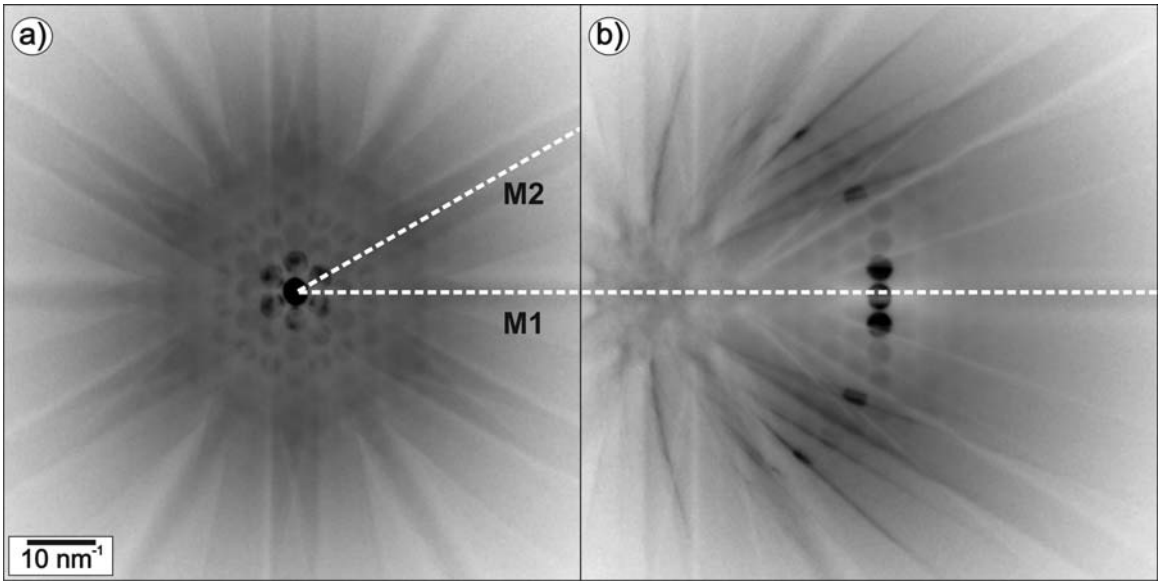

Figure 10: CBED pattern of hexagonal phase showing undisturbed 6mm symmetry. The field of view was extended by tilting the sample along the direction of the symmetry planes (M1, M2) indicated by dashed lines.

In both cases the field of view was extended by tilting the sample along the direction of the symmetry planes indicated by dashed lines. The oval fringes in Figure 9 are an artifact of the in-column energy filter that was used to improve the contrast of the CBED patterns.

The analysis of the symmetry reveals that both phases are characterized by a six-fold rotational symmetry and two independent mirror planes denotes as 6mm symmetry (marked by dashed lines M1 and M2 in Fig. 9(a) and Fig.10(a)) in the zero-order Laue zone (ZOLZ). The 6mm symmetry in the hexagonal phase is not disturbed in the HOLZs. In contrast, the six-fold symmetry is broken in the HOLZs of the plate-like phase. This is visualized for example by the Kikuchi-line pair in Fig. 9(b) (marked by the black dashed lines) which does not show up in Fig. 9(c) for the mirror plane M1' which is equivalent to mirror plane M1. One possible explanation for the symmetry reduction of the plate-like phase could be an alternating stacking of close-packed lattice planes exhibiting cubic and hexagonal structure as recently suggested [7]. This alternating stacking can be analyzed by high-resolution TEM images as shown in Figure 11(a).

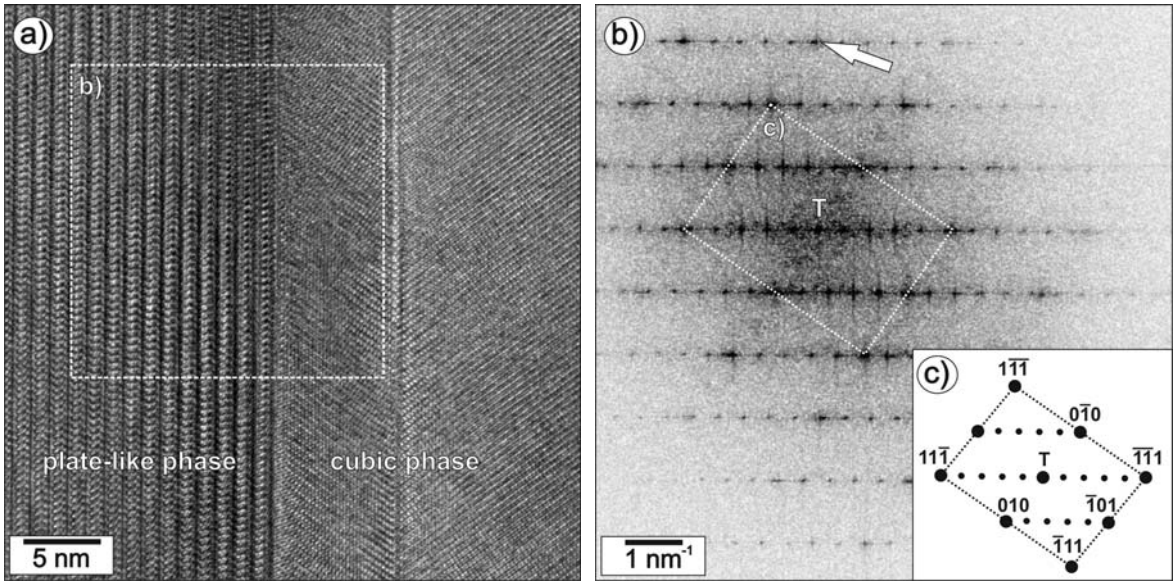

Figure 11: (a) HRTEM image of interface between "plate-like" and cubic phase; (b) diffractograms of the areas marked by the squares; (c) schematic overview of the orientation relation between "plate-like" phase and matrix.

Figure 11(a) shows the interface region between the "plate-like" (left) and cubic phase (right). A twin boundary is observed in the cubic phase close to the interface. A well-defined orientation relationship exists between the plate-like and the cubic phase which is visualized by the Fourier transformation of Fig. 11(a) presented in Fig. 11(b). The dashed lines in Figs. 11(b,c) connect reflections of the cubic phase. The lattice parameter of the plate-like phase in growth direction (1.20 nm) corresponds to the five-fold value of the (111)-plane distance in the cubic phase (0.23 nm). In reciprocal space, this results in a five-fold periodicity of reflections along the [111] direction of the cubic phase as shown in Fig. 11(b,c). The lattice parameters in the interface plane must be considered to understand the orientation relationship between the two phases. The arrow in Fig. 11(b) marks two reflections which belong to the cubic and plate-like phase. The corresponding lattice parameters of 0.16(3) nm and 0.16(4) nm agree well indicating a small lattice-parameter mismatch which explains the orientation relationship between the two phases.

The present study is also concerned with the formation kinetics of hexagonal and plate-like phase [19]. The latter forms quickly (annealing time < 10 h) in the whole temperature range between 700 °C and 900 °C. The "plate-like" phase does not occur at 1000 °C which demonstrates that it is not formed during the cool-down to room temperature. The slow formation of the hexagonal phase at 800 °C requires long annealing times >1000 h.

5. Summary and outlook

$Ba_{0.5}Sr_{0.5}Co_{0.8}Fe_{0.2}O_{3-\delta}$ (BSCF), among all MIEC materials, exhibits excellent oxygen transport properties at high temperatures, thus predestining it especially for oxygen-membrane applications.

In the present report period high-quality epitaxial BSCF nanoscale thin films were, for the first time, deposited on single-crystalline substrates. This facilitated the evaluation of intrinsic electrical conductivity properties as well as oxygen surface exchange coefficients without any influence of grain boundaries present in polycrystalline bulk samples, as used in all studies reported so far in

literature. The resulting oxygen surface exchange coefficients support the outstanding role of BSCF for high-temperature oxygen-transport applications.

Nonetheless, surface exchange kinetics limits the oxygen flux through a dense membrane below a certain thickness. However, before striving for an enhancement of the oxygen exchange kinetics by nanostructured surfaces, a viable means reported for several related MIEC perovskite materials, several issues have to be addressed. So far there has been surprisingly little knowledge on the long-term structural and electrochemical stability under application-relevant conditions. One major drawback of BSCF is an instability of the cubic phase in the operating temperature range of interest (~ 800 °C), resulting in a degradation of electrochemical performance.

In the present reporting period the main focus therefore was on a detailed temperature-phase relationship of BSCF under application-relevant temperatures (700...1000 °C), relating these phenomena to the phase changes observed within the material. The kinetics of the cubic-to-hexagonal phase transition could be determined by long-term XRD analyses of powder samples, revealing hexagonal phase formation at temperatures below ~840 °C and with a time constant $t_{90} \approx 45$ d (at 800 °C).

Besides the verification of the formation of the hexagonal phase, an additional non-cubic phase with plate-like morphology was observed by electron microscopy studies in thin-film and bulk samples. The structure of the "plate-like" phase was analyzed by convergent beam electron diffraction and high-resolution transmission electron microscopy. It consists of regions which are characterized by different stacking of close-packed planes with hexagonal or cubic symmetry. The composition of the "plate-like" phase differs distinctly from the composition of the cubic and hexagonal phases. It forms quickly between 700 ^{o}C and 900 ^{o}C and does not occur at 1000 ^{o}C.

Most recent results reported in literature [21] charted a path forward toward a stabilization of the cubic BSCF phase by suitable cationic substitution strategies. Preliminary studies have shown a suppression of the hexagonal phase at 800 °C. In a next step, while maintaining the favourable cubic phase, a well-defined surface modification with the help of nanostructured functional layers (either nanoporous films of the same material, resulting in an increased electrochemically active surface area, or of a different material enabling a faster oxygen exchange), seems feasible as a well-directed approach to enhance oxygen-transport properties.

References

- own work with complete titles -

[1] Z. P. Shao, W. S. Yang, Y. Cong, H. Dong, J. H. Tong and G. X. Xiong, *Journal of Membrane Science* **172**, 177-188 (2000).

[2] Z. P. Shao and S. M. Haile, *Nature* **431**, 170-173 (2004).

[3] J. F. Vente, S. McIntosh, W. G. Haije and H. J. M. Bouwmeester, *Journal of Solid State Electrochemistry* **10**, 581-588 (2006).

[4] S. McIntosh, J. F. Vente, W. G. Haije, D. H. A. Blank and H. J. M. Bouwmeester, *Solid State Ionics* **177**, 1737-1742 (2006).

[5] S. Švarcová, K. Wiik, J. Tolchard, H. J. M. Bouwmeester and T. Grande, *Solid State Ionics* **178**, 1787-1791 (2008).

[6] M. Arnold, T. M. Gesing, J. Martynczuk and A. Feldhoff, *Chemistry of Materials* **20**, 5851-5858 (2008).

[7] K. Efimov, Q. Xu and A. Feldhoff, *Chemistry of Materials* **22**, 5866-5875 (2010).

[8] B. Wei, Z. Lu, X. Q. Huang, J. P. Miao, X. Q. Sha, X. S. Xin and W. H. Su, *Journal of the European Ceramic Society* **26**, 2827-2832 (2006).

[9] Z. H. Chen, R. Ran, W. Zhou, Z. P. Shao and S. M. Liu, *Electrochimica Acta* **52**, 7343-7351 (2007).
[10] W. Zhou, R. Ran, Z. P. Shao, W. Zhuang, J. Jia, H. X. Gu, W. Q. Jin and N. P. Xu, *Acta mater.* **56**, 2687-2698 (2008).
[11] H. Koster and F. H. B. Mertins, *Powder Diffraction* **18**, 56-59 (2003).
[12] E. Girdauskaite, H. Ullmann, V. V. Vashook, U. Guth, G. B. Caraman, E. Bucher and W. Sitte, *Solid State Ionics* **179**, 385-392 (2008).
[13] E. Bucher, A. Egger, P. Ried, W. Sitte and P. Holtappels, *Solid State Ionics* **179**, 1032-1035 (2008).
[14] M. Burriel, C. Niedrig, W. Menesklou, S. F. Wagner, J. Santiso and E. Ivers-Tiffée, "BSCF Epitaxial Thin Films: Electrical Transport and Oxygen Surface Exchange", *Solid State Ionics* **181**, 602-608 (2010).
[15] C. Niedrig, M. Burriel, S. Taufall, S. F. Wagner, W. Menesklou, S. Baumann and E. Ivers-Tiffée, "Thermal Stability of the Cubic Phase in $Ba_{0.5}Sr_{0.5}Co_{0.8}Fe_{0.2}O_{3-\delta}$ (BSCF)", submitted to *Journal of Membrane Science* (2010).
[16] D. N. Müller, R. A. De Souza, T. E. Weirich, D. Roehrens, J. Mayer and M. Martin, *Physical Chemistry Chemical Physics* **12**, 10320-10328 (2010).
[17] P. Müller, H. Störmer, L. Dieterle, C. Niedrig, E. Ivers-Tiffée and D. Gerthsen, "Determination of phase composition within the $Ba_{0.5}Sr_{0.5}Co_{0.8}Fe_{0.2}O_{3-\delta}$ material system by means of electron microscopy", submitted to *Acta mater.* (2010).
[18] C. Niedrig, S. Taufall, S. F. Wagner, P. Müller, H. Störmer, D. Gerthsen and E. Ivers-Tiffée, "Thermal Stability of mixed ionic-electronic conducting $Ba_{0.5}Sr_{0.5}Co_{0.8}Fe_{0.2}O_{3-\delta}$", in: *Proc. 1st Internat. Conference on Materials for Energy, Karlsruhe/Germany, Book A*, 48-50 (2010).
[19] P. Müller, L. Dieterle, E. Müller, H. Störmer, D. Gerthsen, C. Niedrig, S. Taufall, S.F. Wagner, and E. Ivers-Tiffée, "$Ba_{0.5}Sr_{0.5}Co_{0.8}Fe_{0.2}O_{3-\delta}$ for Oxygen Separation Membranes", *ECS Transactions* **28**, 309-314 (2010).
[20] J.P. Morniroli and J.W. Steeds, *Ultramicroscopy* **45**, 219-239 (1992)
[21] S. Yakovlev, C.-Y. Yoo, S. Fang and H. J. M. Bouwmeester, *Applied Physics Letters* **96**, 254101 (2010)